geosciences

MDPI

Article

Morphological Mimicry in Loess-Mantled Terrains: Re-Evaluating the Quaternary Activity of the Devene Fault

Alexander Radulov *, Yordanka Donkova, Nikolay Nikolov, Marlena Yaneva, Konstantin Kostov and Ivan Alexiev

Geological Institute, Bulgarian Academy of Sciences, 1113 Sofia, Bulgaria; dani@geology.bas.bg (Y.D.); nik69o@abv.bg (N.N.); marlena@geology.bas.bg (M.Y.); kskostov@geology.bas.bg (K.K.); alexiev@geology.bas.bg (I.A.)

* Correspondence: radulov@geology.bas.bg

Abstract

The Devene fault system, a major strike–slip structure at the boundary between the Balkan Range and the Moesian Platform in NW Bulgaria, remains a subject of debate regarding its Quaternary activity. This study investigates the shallow expression of the fault at two representative sites, Tri Kladentsi and Beli Breg, using high-resolution electrical resistivity profiling to differentiate tectonic deformation from climatically driven landscape evolution. At Tri Kladentsi, resistivity profiles confirm a steeply dipping structural boundary within the Miocene bedrock, juxtaposing limestone against sands. The overlying 25 m thick loess cover, however, remains sub-horizontal and undisturbed. Likewise, at Beli Breg, the complex architecture of stacked channel sequences and tributary deposits at the Ogosta River confluence reveals no identifiable fault displacement. Our results suggest a high degree of morphological mimicry, where asymmetric river valleys produced by selective erosion and differential loess accumulation superficially converge with tectonic signatures. The long-term left-lateral slip rate is estimated at 0.14–0.19 mm/yr based on a 20 km Miocene offset. Nevertheless, the lack of modern surface rupture indicates a deceleration of the fault slip rate and a transition to a buried fault top during the Quaternary. These findings necessitate a re-evaluation of regional seismic hazard assessments, because the absence of continuous surface traces physically constrains the maximum earthquake potential.

Keywords: morphological mimicry; tectonic geomorphology; lithological inheritance; electrical resistivity tomography; Devene fault; Moesian platform; Balkan range

Check for updates

Academic Editor: Rosa Nappi

Received: 20 March 2026
Revised: 22 April 2026
Accepted: 28 April 2026
Published: 2 May 2026

Copyright: © 2026 by the authors. Licensee MDPI, Basel, Switzerland. This article is an open access article distributed under the terms and conditions of the Creative Commons Attribution (CC BY) license.

1. Introduction

The Devene fault system was initially characterized through extensive hydrocarbon exploration along the transition zone between the Balkan Range and the Moesian Platform in NW Bulgaria (Figure 1). Although its deep-rooted structural architecture is documented [1–3], its classification as an active Quaternary fault continues to be a matter of debate. Assessing the seismogenic potential of the Devene fault is critical for infrastructure safety, specifically regarding its proximity to the Kozloduy Nuclear Power Plant and the geomechanical integrity of feasible carbon capture and storage reservoirs within the platform. Currently, the paucity of fault data and near-surface structural evidence represents a primary impediment to robust seismic hazard assessment and the implementation of effective risk mitigation strategies.

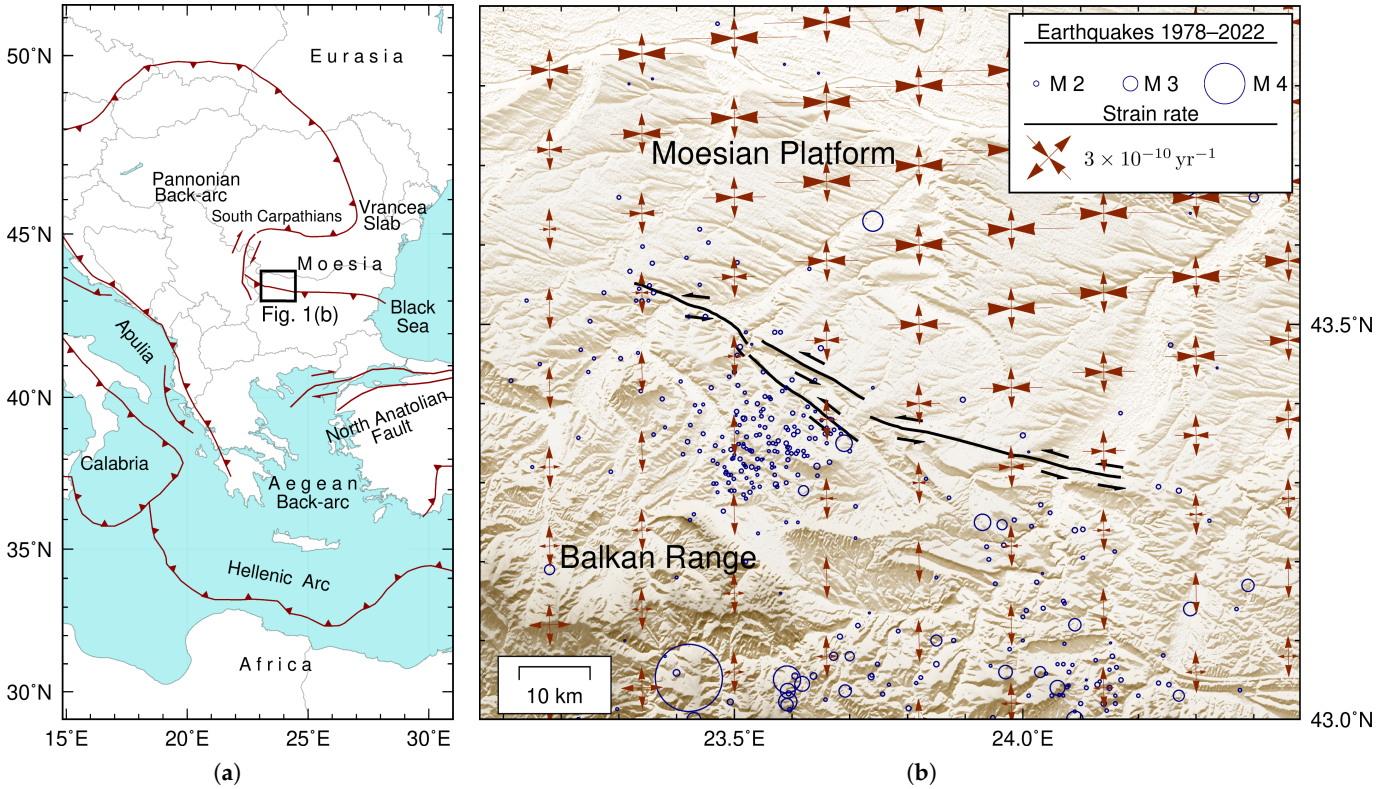


Figure 1. Locality map of the study area: (**a**) Regional tectonic setting of the Balkan–Carpathian region. Geodynamic map illustrating the interaction between the Eurasia and Africa plates. The Moesian Platform acts as a rigid block situated between the South Carpathians and the Balkan Range. The tectonic evolution is dominated by the eastward retreat of the lithospheric slab beneath the Carpathians. (**b**) Local seismotectonic setting and present-day kinematics of the Devene fault system. In the western sections of the Moesian platform and the Balkan range, the explicit contrast strain rate field (geodetic data from [4]; horizontal principal axes of the strain rate field from GNSS data are shown by red arrows) suggests that the orogen–platform transition represents an active tectonic boundary. Digital elevation data from [5], seismicity from [6].

On a regional scale, Balkan geodynamics are driven by Eurasia–Africa convergence (Figure 1a), specifically the northward movement of the African plate and the indentation of the Adria–Apulia microplate [4,7–9]. This interaction facilitates complex microplate rotations and back-arc extension, further influenced by the "slab pull" of the descending Vrancea lithospheric block to the north [10]. Although the Moesian Platform acts as a stable foreland, it nonetheless has the potential to accommodate intraplate deformation along inherited structural discontinuities. The Devene fault system serves as an example of such a feature, marking the transition between the platform and the Balkan Range where contemporary regional stresses may trigger reactivation. Despite these clear geodynamic drivers, the specific kinematic expression and activity of the fault system remain poorly constrained.

Data regarding the Devene fault, including its surface features, geometry, kinematics and timing, are inconsistent and often based on hypothetical models that lack thorough field validation. Current seismic hazard assessments rely on regional databases that characterize the western fault segment as a strike–slip source capable of $M_w \approx 7.2$ events, whereas a portion of the eastern segment is interpreted as a normal fault capable of $M_w \approx 6.5$ [11,12]. Recent high-resolution geophysical investigations into shallow Quaternary fluvial successions found no evidence of surface rupture at an eastern site [13] and identified only potentially tectonically disturbed sediments within the central sector [14] (Figure 2). Given

that nearly half of the fault system remains data-deficient, we conducted this pilot study to characterize the geomorphology and shallow subsurface architecture at two representative sites along the western segment of the Devene fault.

The Devene strike–slip fault system consists of two primary segments, each approximately 35 km in length (Figures 1 and 2). The system maintains an average strike of 112° and dips steeply 70–80° [15] to the SSW [1,2], extending to a crustal depth of approximately 15 km [15]. The eastern fault segment is characterized by a discrete, linear trace constrained by deep seismic reflection profiles and borehole data obtained from between the Skat and Iskar valleys (Figure 2) [1–3,16]. The western segment exhibits a more complex, bifurcated architecture comprising two sub-parallel branches that converge toward the WNW. The southern (rear) fault branch is topographically expressed as a fault line and was initially identified in outcrop [17]. Conversely, the northern (front) fault branch remains blind or buried, having been traced to the sub-Quaternary unconformity primarily through field geophysics and borehole datasets [1–3,18].

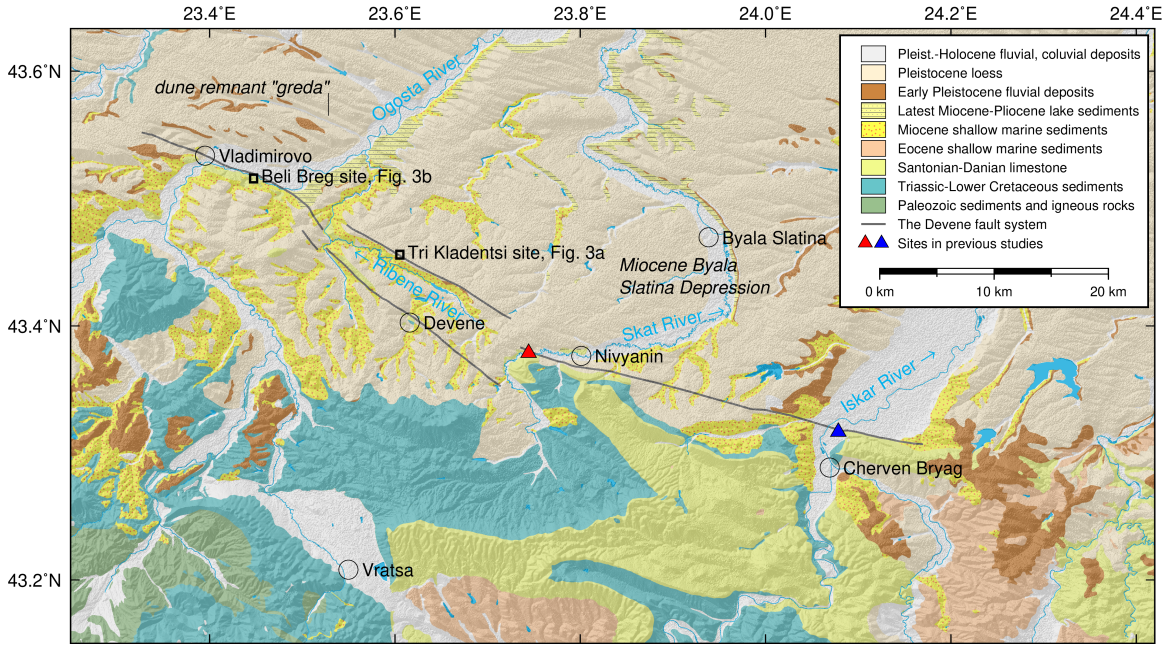


Figure 2. Simplified geological map of the Devene fault system region. Indicated field sites include Tri Kladentsi (Figure 3a) and Beli Breg (Figure 3b), alongside published reference locations in the Iskar floodplain showing no evidence of Quaternary activity [13] (a blue triangle) and the Skat floodplain exhibiting tectonically disturbed sediments [14] (a red triangle).

The upthrown block of the Devene fault system comprises an uplifted Mesozoic basement that forms a structural and topographic culmination relative to the subsiding depocenters to the north (Figure 2). This southern block exposes a deformed Upper Cretaceous–Paleogene carbonate sequence that underwent significant erosion prior to burial by Neogene and Quaternary successions. The stratigraphic framework of the Campanian–Danian interval (ca. 84–62 Ma) includes five lithostratigraphic units [19]: the siliciclastic–carbonate transition of the Novachene Formation (sandstones and marls); sandy limestones of the Darmantsi Formation; argillaceous limestones of the Kunino Formation; chert-bearing limestones of the Mezdra Formation; and the limestones of the Kaylaka Formation. These units unconformably overlie Albian siliciclastics (marls, shales, and sandstones) of the Malo Peshtene and Roman Formations [20,21]. The Mesozoic–earliest Paleogene strata exhibit a structural style dominated by sub-horizontal thrust nappes with characteristic flat–ramp–flat geometries [14], originating during Eocene crustal shortening [22]. The Devene fault subsequently intersected these pre-existing thrust sheets. The development of a younger

strike–slip system along the boundary between the Moesian Platform and the Balkan Range is consistent with the regional tectonic evolution. The Moesian Platform, acting as a rigid Eurasian fragment, was indented between the South Carpathians and the Balkan Range (Figure 1a). This indentation was driven by the eastward slab retreat beneath the Carpathians during the Oligocene–Miocene [23]. The deformed bedrock is unconformably draped by Miocene siliciclastic–carbonate sediments deposited in shallow marine facies [24]. The Miocene successions exhibit thickness variations and facies distributions [3,25–27], indicating that the Devene fault was active during Miocene deposition and controlled the local accommodation space. The marine successions are overlain by Pliocene lacustrine deposits and a prograding continental sequence of Villafranchian age (late Pliocene–early Pleistocene) [28]. These fluvial gravels and sands prograded primarily toward the north and northeast, reflecting the transport of coarse clastic material from the rising Balkan orogen. These deposits constitute a primary geomorphic paleo-surface and mark the initial subaerial emergence and incision of the paleo-Danubian drainage system [29]. The transition was driven by the interplay of regional tectonic uplift of the Moesian Platform and the subsequent base-level drop associated with the eastward retreat and eventual drainage of the Dacian Lake toward the Black Sea basin [28]. Finally, the low-relief interfluvial surfaces across the region are mantled by an extensive Quaternary loess cover, which obscures much of the underlying structural complexity [28–30]. The Devene fault serves as an important kinematic boundary within the contemporary strain field that marks the transition from orogenic extension in the south to platformal shortening to the north (Figure 1b) [4,31]. This kinematic transition suggests that the Devene fault accommodates modern crustal deformation, despite an absence of documented historical seismicity in its immediate vicinity. Background seismicity in the region (Figure 1b) is largely confined to shallow crustal levels, occurring above a low-velocity layer situated at approximately 10 km depth [15]. However, the nature of the contemporary tectonic landscape remains a subject of debate. Several authors [32–34] have interpreted the presence of linear, high riverbanks within asymmetric valleys as diagnostic tectonic features indicative of neotectonic vertical displacement. In the Iskar Valley, Vaptsarov et al. [35] documented a 30–40 m vertical displacement of the Villafranchian level and attributed this displacement to activity along the Devene fault since the onset of the Quaternary. Despite these geomorphological arguments, traditional geological studies have yet to produce conclusive evidence of ruptured Quaternary fluvial or loess sediments. Furthermore, it is noteworthy that the study area lacks secondary indicators of Quaternary faulting, such as fault-related travertines, tufas, or sinkhole alignments. This lack of primary and secondary structural evidence in the youngest stratigraphic markers highlights the need for high-resolution subsurface imaging to distinguish between purely climatically driven fluvial incision or specific loess morphologies and active tectonic deformation.

Given the conflicting interpretations between geomorphological proxies and the lack of documented surface ruptures, the primary aim of this study is to determine the nature of Quaternary deformation along the western segment of the Devene fault. We first utilize high-resolution electrical resistivity profiling at the Tri Kladentsi and Beli Breg sites (Figure 3) to investigate whether deep-seated structural boundaries propagate into the overlying loess and fluvial successions. Building on this subsurface data, we re-evaluate the origin of regional asymmetric valleys and linear riverbanks to test whether these features represent true tectonic displacement or are pseudo-tectonic landforms driven by eolian processes and dominant paleowind patterns. This investigation provides field-validated constraints on fault behavior, specifically addressing the transition from long-term Miocene fault slip to potentially blind or distributed modern deformation, in order to refine the maximum earthquake potential for regional seismic hazard models. By bridging the gap

between deep-seated structural maturity and near-surface expression, this pilot study seeks to clarify the role of the Devene fault as a potential hidden seismic source within the Moesian Platform.

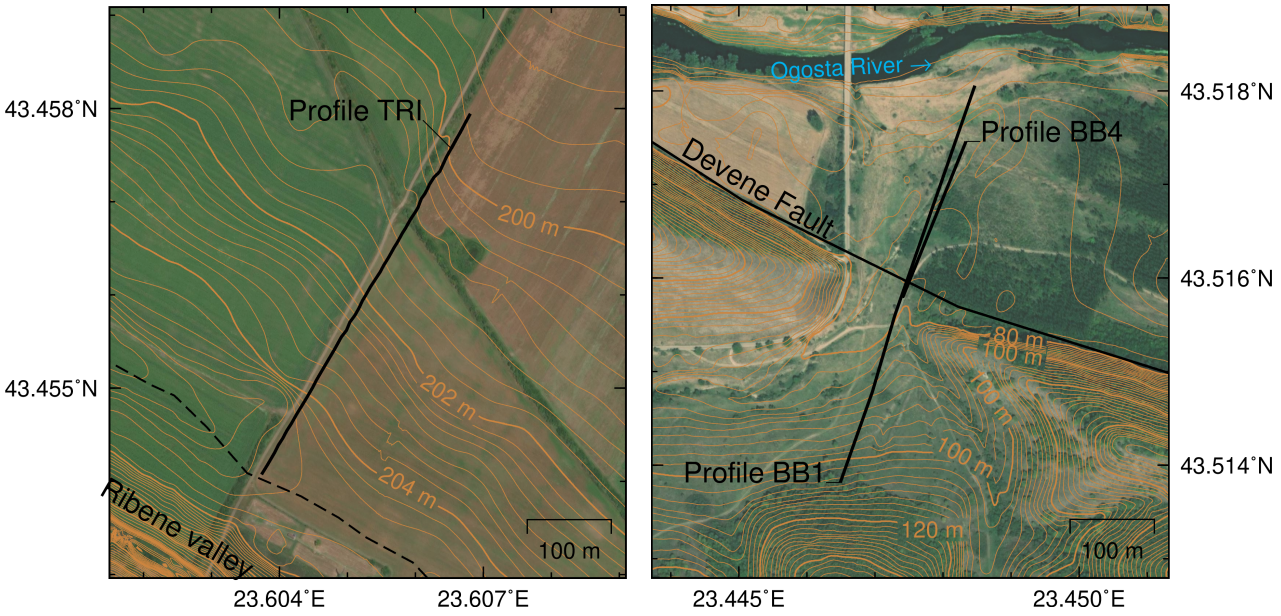


Figure 3. Detailed site map displaying Microsoft Corporate® Bing™ satellite images, topography and layout of the geophysical survey at the study areas: (**a**) Tri Kladentsi site, with 0.25 m contour intervals and the drainage divide indicated by a dashed line; (**b**) Beli Breg site, with 2 m contour intervals.

2. Site Selection

We selected two study sites representative of the dominant geomorphic and depositional environments in the region to investigate the shallow expression of the Devene fault. The Beli Breg site characterizes linear fluvial reaches formed downstream of fault intersections, oriented parallel to the paleo-wind direction during loess accumulations. Conversely, the Tri Kladentsi site represents a loess-mantled upland environment.

2.1. Tri Kladentsi: Upland Loess

The Tri Kladentsi site is situated within the central sector of the western segment, where the fault system bifurcates (Figure 2). The Ribene River occupies a rectilinear valley between these fault branches, likely exploiting a zone of mechanical weakness within the Miocene limestone. The southern fault branch is clearly exposed at Devene village, juxtaposing Upper Cretaceous and Miocene successions within a distinct fault breccia zone. In contrast, the northern fault branch is blind and characterized only through subsurface data [16].

A defining feature of the selected site is the extreme topographic asymmetry: the northern (right) valley slope coincides with a watershed, resulting in a severely restricted northern catchment of the Ribene River (Figure 3a). This inhibited northward drainage expansion suggests that tectonic uplift along the northern fault branch may function as a structural barrier. To investigate whether this structure displaces Quaternary strata in the shallow subsurface, electrical resistivity profile TRI was positioned across the upland, extending from the drainage divide (Figure 3a).

2.2. Beli Breg: River Confluence

The Ogosta River intersects the western tip of the Devene fault system. Downstream of this junction, the river has carved an asymmetric valley (Figure 2) aligned with the dominant wind direction prevalent during Quaternary aeolian deposition [28,30,36]. Subsurface borehole data initially identified a buried fault at the base of the southern valley slope, interpreted as a reverse fault [16]. However, consistent with the transcurrent setting, the fault is characterized as a steeply dipping structure [15]. Subsequent studies have characterized this structure as an active fault at the same location [32,33,35].

The Beli Breg site sits at the confluence of the Ogosta and a short tributary that incised the high limestone bank to the south (Figure 3b). This location is unique, as it represents the only structural reach where a relatively thick Quaternary sequence has accumulated on the upthrown fault block. Two resistivity profiles were deployed here: BB1, providing a regional view across the tributary valley and Ogosta floodplain, and BB4, utilizing a higher electrode density to resolve the complex lateral transitions that were identified in the initial survey.

3. Methods

Among various geophysical techniques, electrical resistivity profiling is a well-established method for the preliminary characterization of the shallow subsurface. It is particularly effective for identifying fault rupture traces across diverse depositional and tectonic settings [37–43]. The application of high-resolution resistivity profiling to identify buried structural discontinuities follows established workflows for active fault detection in complex sedimentary settings, e.g., [44]. The method involves injecting a controlled electrical current into the ground and measuring the resulting potential difference through surface electrodes to map the subsurface resistivity distribution. For this study, resistivity measurements were collected using single-channel Terrameter SAS 1000 (ABEM, Sundbyberg, Sweden) equipped with an automated electrode switcher. The survey configuration utilized four 100 m-long multicore cables (ABEM, Sundbyberg, Sweden) and a total of 81 stainless steel electrodes (custom-made by the authors' institution). Geophysical investigations were conducted at two study sites, Tri Kladentsi and Beli Breg, and were designed to optimize the detection of fault-related anomalies by utilizing different electrode configurations and spatial resolutions tailored to the specific site conditions (Table 1).

Table 1. Acquisition parameters for the electrical resistivity surveys conducted at the Tri Kladentsi and Beli Breg sites. The table details the specific electrode arrays, spatial resolutions (minimum electrode spacing), total profile lengths and the topographic measurement techniques employed for each transect.

Site	Profile	Array Protocol	Min. Spacing	Total Length	Topo Method
Tri Kladentsi	TRI	Gradient	10 m	500 m	Laser Level
Beli Breg	BB1	Dipole–Dipole	10, 5 m	500 m	GNSS-RTK
Beli Breg	BB4	Wenner–Schlumberger	4, 2 m	200 m	GNSS-RTK

Geophysical investigation at the Tri Kladentsi site was conducted along profile TRI, utilizing a 500 m-long transect. A Gradient array was selected for its sensitivity to lateral and vertical resistivity variations [45,46]. A 10 m minimum electrode spacing was maintained to balance the depth of investigation with lateral sensitivity. To achieve the total 500 m length, a roll-over technique involving two station shifts was employed, ensuring seamless data continuity across the entire profile. Topography was recorded using a laser leveling device (Parkside, Neckarsulm, Germany).

Investigations at the Beli Breg site utilized a multi-scale approach with two profiles of varying resolutions to pinpoint the expected fault zone. Profile BB1 was measured using a Dipole–Dipole array to maximize sensitivity to lateral changes [45,46]. A dual-spacing approach was used, incorporating both 10 m and 5 m minimum electrode spacings. The profile reached a total length of 500 m. To enhance resolution in the central portion where the fault was anticipated, two roll-over stations were positioned strategically between the 2nd and 3rd cables, and the 3rd and 4th cables. Following the initial findings from profile BB1, profile BB4 was positioned across a specific lateral transition to provide a higher-resolution image of the subsurface. The protocol was reverted to a Wenner–Schlumberger array for structural detail. This electrode configuration was selected for its superior sensitivity to both horizontal and vertical structures [45,46], making it particularly appropriate for identifying the high-angle stratigraphic displacements and resistivity contrasts typically associated with fault ruptures. Higher-density sampling was achieved using 4 m and 2 m minimum electrode spacings. A total length of 200 m was covered. Likewise in profile BB1, the roll-over technique was applied with two station shifts to ensure high data density in the target zone. Topographic corrections were derived from GNSS-RTK (Global Navigation Satellite System-Real-Time Kinematic) measurements using a Topcon GR-3 receiver (Topcon Corporation, Tokyo, Japan).

The raw apparent resistivity data were inverted using the Boundless Electrical Resistivity Tomography (BERT v.2.2) software package, utilizing a Gauss–Newton algorithm with global regularization [47,48]. BERT employs unstructured triangle meshes for 2D forward modeling, facilitating precise terrain correction by incorporating surface topography into the mesh. The resistivity models were refined by adjusting the regularization parameter (λ), which controls the trade-off between data fit and model smoothness, and the anisotropic regularization, which defines the relative weight of vertical versus horizontal boundaries.

For profile TRI, a consistent λ of 20 was used to evaluate the subsurface through two distinct modeling objectives. The first model employed a vertical constraint of 0.2 to characterize the layered medium. The second model utilized a significantly higher vertical constraint of 2.0 to resolve vertical heterogeneity, thereby enhancing the visibility of potential fault planes and lateral resistivity contrasts.

The inversion parameters were determined using the L-curve criterion to balance the trade-off between data fit (misfit) and model roughness [47]. For the reconnaissance profile BB1, an initial λ of 320 was selected, decreasing by 50% across 6 iterations. The high-resolution profile BB4 utilized a higher initial λ of 640 with a more gradual reduction of 25% over 11 iterations. The optimum starting λ values were identified using the automated optimization routine (LAMBDAOPT) within the BERT v.2.2 software package. Furthermore, both profiles were modeled using a vertical constraint of 0.2, effectively simulating a layered medium to highlight potential stratigraphic offsets.

4. Results and Interpretation

Geophysical results from the Tri Kladentsi and Beli Breg sites image the shallow subsurface architecture with a high resolution that enables a critical evaluation of fault activity during Quaternary times.

4.1. Resistivity Profile at Tri Kladentsi Site

The subsurface architecture at the Tri Kladentsi site was interpreted by evaluating two complementary resistivity models to ensure structural consistency (Figure 4). Although both tomograms display a comparable overall resistivity distribution, incorporating distinct vertical anisotropy factors during the inversion process allows for a more robust characterization of the three primary subsurface zones.

The uppermost unit across the entire profile is characterized by a conductive signature (≤23 Ωm; Figure 4) that is typical for loess deposits. The low resistivity values recorded within the uppermost Quaternary unit are characteristic of wet clayey loess, consistent with the regional lithostratigraphy described by Minkov [30]. This high conductivity is attributed to the combined effect of high clay content, which is typical for the periphery of the Moesian Platform [29,30,36], and increased seasonal water saturation. Such values provide a sufficiently distinct electrical contrast with the underlying high-resistivity bedrock, allowing for a high-confidence assessment of the contact geometry. This loess unit maintains a consistent average thickness of approximately 25 m. At the southern terminus, the base of the loess is situated at an elevation of ∼185 m, which correlates precisely with the elevation of the limestone–loess contact observed in the adjacent valley.

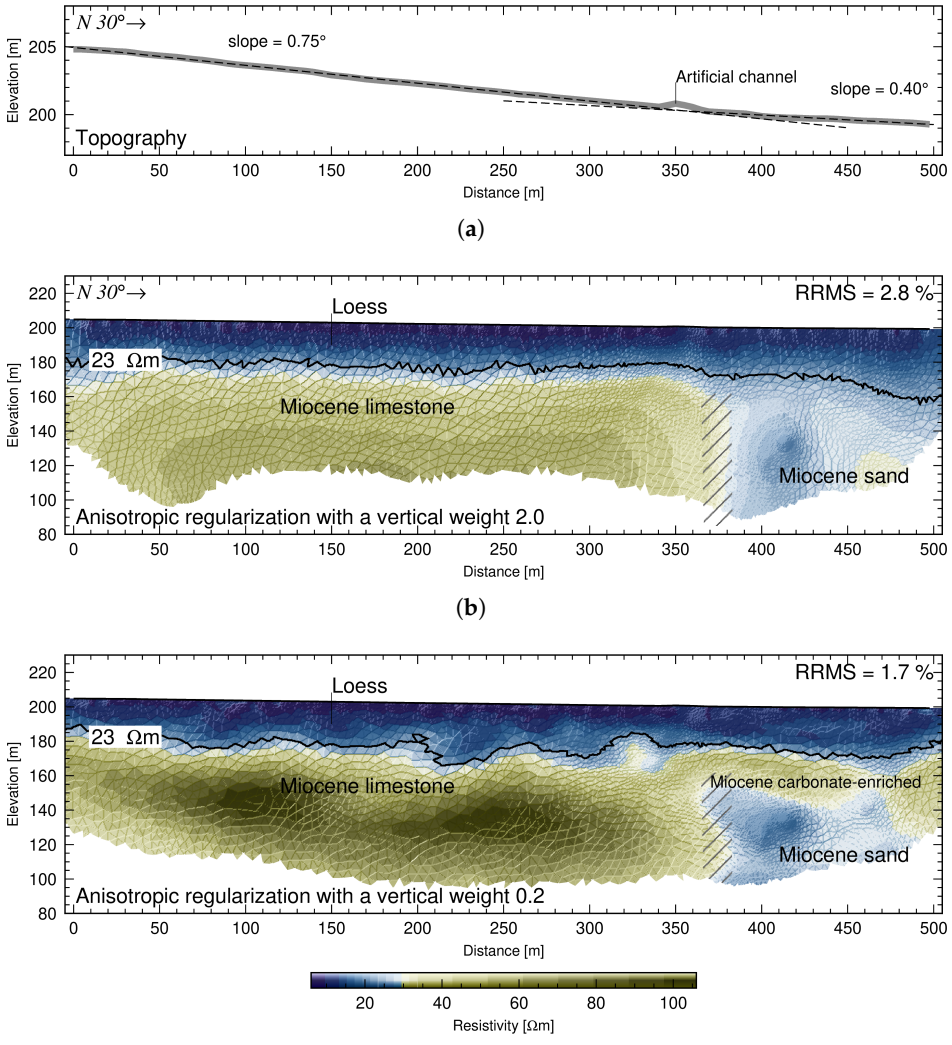


Figure 4. Electrical resistivity results for profile TRI at the Tri Kladentsi site, comparing different anisotropic regularization weights. (**a**) Topographic profile exhibiting a gentle slope and a subtle topographic flexure. (**b**,**c**) Resistivity inversion models utilizing an anisotropic triangular mesh constrained by topography. The subsurface is interpreted as a layered system comprising loess (marked by a bold 23 Ωm contour), Miocene limestone and Miocene sand. The hatched area in (**b**,**c**) delineates the lateral transition zone between the limestone and sand units. (**b**) Model result using an anisotropic vertical weight of 2.0. This configuration emphasizes vertical heterogeneity, resulting in a more blocky structure in the central portion, with a relative Root Mean Square (RRMS) error of 2.8%. (**c**) Model result using an anisotropic vertical weight of 0.2. This setting favors horizontal stratification, yielding more continuous units and a lower RRMS error of 1.7%.

To ensure the robustness of our interpretation, we compared two contrasting inversion models (Figure 4b,c) to assess the sensitivity of the results to different regularization constraints. The tomograms indicate that the Miocene limestones exposed on the nearby valley slope extend northward beneath the loess cover, forming a zone of relatively high resistivity. The observed resistivity values vary based on the inversion constraints: 40–70 Ωm in the model with a 2.0 vertical anisotropy factor (Figure 4b), which in our BERT configuration emphasizes vertical heterogeneity and yields a more blocky structure, and 40–110 Ωm in the model with a 0.2 factor (Figure 4c), which favors horizontal stratification and yields more continuous units. Beneath the loess in the northernmost section, resistivity values decrease to approximately 20 Ωm. This low-resistivity zone is interpreted as Miocene sediment, likely comprising sand layers capped by a carbonate-enriched horizon. A distinct lateral transition is observed between the Miocene limestones and the more conductive Miocene siliciclastics. This transition is confined to a vertical zone approximately 10 m wide, positioned between the 370 m and 380 m marks on profile TRI (Figure 4). The high-angle nature of this boundary, persistently resolved across both weighting schemes but more sharply defined in the 2.0 anisotropy model (Figure 4b), suggests a structurally controlled contact interpreted as a steeply dipping fault zone.

The almost vertical transition zone identified at the Tri Kladentsi site is consistent with a strike–slip fault, e.g., [49,50]. This interpretation could explain the juxtaposition of distinct Miocene sedimentary sequences, limestone to the south and sand to the north, as a likely result of lateral fault displacement. Although the exact morphology of the loess base varies slightly depending on the used resistivity model, the erosional surface across both Miocene units remains sub-horizontal, which suggests that any vertical fault displacement following the onset of aeolian deposition is either negligible or below the detection limit of the survey.

Nevertheless, minor vertical displacement cannot be entirely dismissed, particularly given the subtle topographic flexure observed directly above the inferred fault trace (Figure 4a). This slight 0.35° shift in topographic slope may represent primary tectonic deformation or, more likely, differential loess settlement. Such settlement is frequently driven by selective hydroconsolidation [51,52], a process well-documented in the metastable loess of the Moesian Platform [30]. This effect is likely amplified at this location by the contrasting permeability of the underlying Miocene units, which facilitates localized moisture ponding and subsequent fabric collapse. The intrinsic vertical and horizontal heterogeneity of the loess complex in Northern Bulgaria plays a decisive role in such landscape development; as highlighted by Evstatiev and Antonov [53], high porosity and collapsibility often result in the formation of relief lowerings and “steppe limpits” that are easily misinterpreted as tectonic depressions. Furthermore, the anisotropic texture and variable moisture regime within the unsaturated loess zone [54] can induce differential compaction and surface subsidence, directly contributing to the morphological mimicry observed across the Devene fault zone. In this model, the inherited basement architecture dictates localized drainage patterns within the overburden, triggering heterogeneous hydro-mechanical responses in the loess. Even if the observed topographic shift is interpreted as tectonic, the resulting cumulative displacement remains minimal and insufficient to characterize the Devene fault as a primary Quaternary surface-rupturing structure.

4.2. Resistivity Profiles at Beli Breg Site

The resistivity models BB1 and BB4 reveal two distinct units at depth, overlain by subhorizontal layers of varying resistivity (Figure 5). The high-resistivity bedrock (150–1000 Ωm) represents Upper Cretaceous limestones, whereas the low-resistivity unit (13–140 Ωm) is interpreted as the Miocene Dimovo Formation, comprising sand, sand-

stone, and detrital limestone [24]. The lateral contact between these two units suggests an erosional paleoslope rather than a fault. While profile BB1 reveals a subvertical to south-dipping contact below 30 m that likely indicates a deeper fault, the gradual resistivity transition within the overlying Miocene sediments suggests that this structure does not propagate into the younger strata. A localized conductive anomaly is observed between 90–130 m. This feature is interpreted as a primary lithological variation within the Miocene sand bedrock, possibly representing an infilled paleo-channel or an argillaceous lens. Crucially, the overlying Quaternary units remain sub-horizontal and drape this concave geometry, suggesting that the feature is an inherited stratigraphic element of the Miocene basement and not a result of Quaternary tectonic subsidence or faulting.

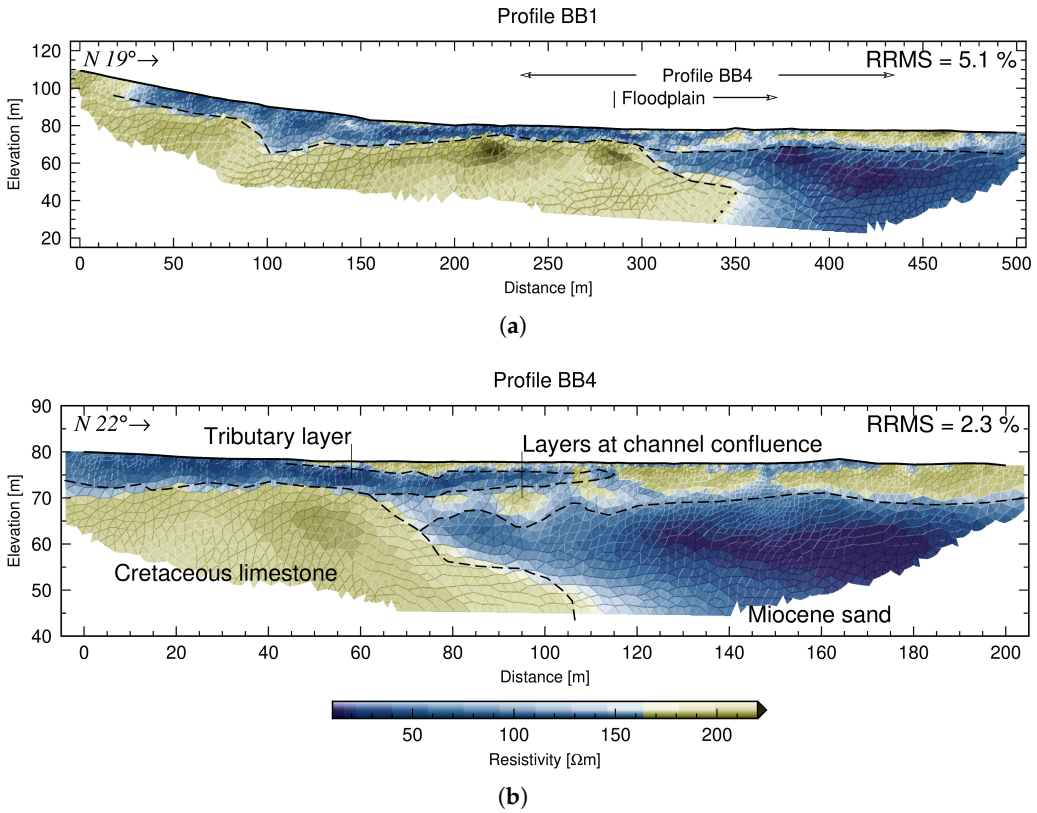


Figure 5. Electrical resistivity results for the Beli Breg study site. (**a**) Profile BB1: A 500 m long reconnaissance resistivity profile providing a regional view across the tributary valley and Ogosta floodplain. The model illustrates the transition from high-resistivity Cretaceous limestone to lower-resistivity Miocene and Quaternary successions. Dashed lines delineate the stratigraphic contacts between Cretaceous limestone, the Miocene Dimovo Formation, and Quaternary cover; the dotted line indicates an inferred subvertical to south-dipping fault below 30 m depth. (**b**) Profile BB4: A 200 m high-resolution profile positioned to resolve the complex lateral contact between the Cretaceous limestone and the Miocene sand. The interpreted dashed lines highlight the tributary layer and the stacked channel sequences within the flow deflection zone. The lack of sharp vertical offsets in the Quaternary strata suggests that the observed subsurface complexity is driven by hydrodynamic confluence dynamics rather than active tectonic displacement.

The deeper units are unconformably overlain by a Quaternary sequence of subhorizontal layers. These strata exhibit significant lateral and vertical resistivity variations, suggesting accumulation under long-term confluence dynamics. This environment was likely characterized by the lateral migration of tributary junctions and mainstream channels, which produced highly heterogeneous depositional patterns. The overall geometry and prevalence of high-resistivity layers suggest an influence from alluvial fan development, where sediment-saturated tributary flows prograded into the trunk valley. Specifically, the

layers at the channel confluence exhibit a stacking pattern reminiscent of oblique aggradation and fluvial channel-fills [55]. This architecture is consistent with a local base-level rise that triggered aggradation of the main trunk and the subsequent lateral progradation or avulsion of the tributary. High resistivity values beneath the floodplain (110–690 Ωm) indicate the presence of coarse-grained material, correlating with the poorly sorted sediment and abundant limestone cobbles observed at the surface. The accumulation of coarse limestone particles stands in stark contrast to the silt-dominated deposits found upstream of the Ogosta River. The stratigraphy reveals a tributary-dominated depositional regime, consistent with an alluvial fan, where the main river lacked the hydraulic competence required to transport the coarse clasts delivered by the tributary. The base of this high-resistivity unit onlaps the limestone bedrock, while its upper extent surpasses the limestone boundary to coincide with the edge of the modern floodplain. The high-resolution imaging of the flow deflection zone, situated directly above the deep contact between the Cretaceous limestone and Miocene sediments, shows these stacked channel sequences. These stratigraphic features exhibit a continuous geometry without any identifiable fault displacement.

Lower resistivity values (25–100 Ωm) define a single tributary layer that is exposed on the surface to the south. The decrease in resistivity is likely attributable to high concentrations of sands derived from proximal Miocene outcrops. The interdigitation of pure tributary deposits within the broader confluence sequence records periods of progradation, likely driven by either intensified alluvial fan activity or a reduction in the discharge of the trunk stream. Crucially, this tributary-derived layer shows no signs of structural disruption. It preserves a continuous geometry consistent with the broader Quaternary record, effectively precluding any notable fault-related displacement at this location.

We attribute the structural complexity of the Quaternary layers to the migratory history of the flow deflection zone rather than tectonic deformation. The strata lack the sharp vertical offsets or discrete discontinuities typical of fault rupturing. Instead, the sedimentary architecture records the maximum landward retreat of the confluence, representing a long-term hydrodynamic boundary structurally anchored at the pre-existing limestone–sand contact.

5. Discussion

The geophysical survey results confirm with high certainty the presence of a fault within the Miocene sediments. However, robust evidence for fault deformation during the Quaternary remains elusive. Observed lateral variations in the younger strata are better explained by non-tectonic factors, such as confluence facies and selective hydroconsolidation of the loess, the locations of which were likely controlled by the contrasting lithologies juxtaposed on either side of the fault. The morphological features of the Devene fault area are more robustly explained by a combination of Quaternary climatic forcing and the structural architecture inherited from earlier tectonic phases. The sedimentary evolution of the Balkan–Carpathian basins is strongly influenced by the composition and mechanical properties of the underlying Mesozoic basement, which dictates the localization of modern fluvial systems and surface landforms through lithological inheritance rather than active crustal deformation. Potential Quaternary fault activity warrants continued consideration, as its characterization is fundamental to a robust seismic hazard assessment. If the displacement on the Devene fault is predominantly lateral, any associated vertical component may remain below the resolution thresholds of the geophysical methods employed. Because our profiles are oriented perpendicular to the fault strike, pure strike–slip motion would be identifiable through the lateral juxtaposition of contrasting electrical properties or discrete vertical discontinuities within the Quaternary section [56,57]. No such diagnostic features were identified in the acquired data. Therefore, we suggest a lack of notable strike–slip

surface rupture. Consequently, the lack of expression in the geophysical profiles reinforces the model of a buried fault, e.g., [1,2,11,12,16], and challenges previous assertions regarding the presence of well-defined tectonic landforms, e.g., [32–35].

5.1. Morphological Mimicry: Eolian and Fluvial Controls

Identifying tectonic landforms associated with the Devene fault is complicated by high erosion rates and pervasive loess deposition. Since Marine Isotope Stage (MIS) 22 (ca. 1.03 Ma) [29], aeolian processes dominated landscape evolution and led to a marked morphological convergence between aeolian features and tectonic structures. An important example of this phenomenon is the development of asymmetric valleys, which superficially mimic the surface expression of fault deformations. The prevailing paleowind orientation, steered by regional topography, drove differential deflation and loess accumulation, governing the asymmetric morphology of the three major river valleys that intersect the Devene fault system.

The reaches of the Ogosta, Skat, and Iskar Rivers within the Moesian Platform exhibit pronounced valley asymmetry sensitive to the orientation of the river course relative to the W–WNW prevailing paleowinds [28,30,36]. In the western Moesian Platform, river reaches oriented perpendicular to the wind direction display steeper windward slopes. This asymmetry is attributed to preferential loess accumulation on the leeward banks, which forced a systematic eastward migration of active channels and subsequent lateral erosion of the windward slopes [30].

Local evidence for this paleowind regime is preserved in the form of longitudinal loess dunes, or "gredas" (an example is shown in Figure 2). These are relict features elongated parallel to the wind direction, extending up to 40 km in length and 300–1200 m in width, and rising 20–40 m above adjacent dry gullies [30,58]. Within the western Moesian Platform, the longitudinal axes of these dunes align at 110–120° azimuth (Figure 2b). This orientation confirms that the paleowind direction in the vicinity of the Devene Fault was consistent with the regional WNW flow, providing a mechanical basis for the observed valley migration [28,30]. Where the river reaches align with the Devene fault, they deflect eastward into WNW–ESE courses characterized by linear, high-relief right banks incised into resistant Upper Cretaceous limestones, while the floodplains broaden northward into erodible Neogene sedimentary successions (Figure 2).

Previous investigations have attributed this channel deflection at the intersection with the Devene Fault to active tectonic forcing, e.g., [32,33,35]. Our findings however suggest that these features result from selective erosion across lithological contacts. In this model, disproportionate loess aggradation on leeward surfaces drove eastward river inflections independently of modern fault activity. This is a process of "mimicry" noted in European loess terrains where wind-driven orientations often override or mask the structural fabric [59,60]. Crucially, our geophysical surveys, consistent with the results of Radulov et al. [13] for the Iskar floodplain (see Figure 2), showed no discrete fault-related deformation within the shallow Quaternary strata. The lateral continuity of the observed lithostratigraphic units across the projected fault strike suggests that high rates of sedimentation and fluvial reworking have either obscured any minor tectonic signal or, more likely, indicate a period of Quaternary stasis for this segment of the Devene fault. These results contrast with previous morphostructural interpretations of significant fault subsidence during the Quaternary [35].

The reported 30–40 m displacement of ancient river terraces, originally interpreted as tectonic by Vaptsarov et al. [35], remains unsupported by absolute geochronology. No dated stratigraphic markers exist to confirm a tectonic offset of the elevated fluvial deposits. The regional correlation of these levels relies primarily on Villafranchian mammal

zones (MNQ 16–MNQ 18) [61], which represent broad biochronological units spanning approximately 3.6 to 1.2 Ma [62]. Such million-year-scale intervals lack the temporal resolution required to distinguish between Quaternary tectonic displacement and long-term landscape evolution. This chronological ambiguity is a known issue. For instance, Ruszkiczay-Rüdiger et al. [63] used ^{10}Be cosmogenic nuclide dating on Danube terraces to demonstrate that vertical landscape features can be difficult to interpret. They argued that the terrace staircase resulted from an interplay between uplift and climate change, where the differential preservation of terrace remnants, formed during distinct glacial–interglacial cycles, can create complex geometries that might otherwise be misinterpreted as simple tectonic offsets. In the absence of similar high-resolution geochronological and subsurface structural confirmation for the Devene fault, these geomorphic features are more robustly interpreted as products of non-tectonic factors rather than active Quaternary surface rupture.

5.2. Regional Context and Segmented Activity

To date, the only documented evidence of near-surface coseismic deformation is localized within the Skat River floodplain, situated at the western termination of the eastern segment of the Devene fault system [14]. High-resolution electrical resistivity profiling in this sector identified deformed fluvial successions, which are interpreted as manifestations of strain distributed across a broad damage zone; see Figure 2 [14]. This deformation contrasts with the regional lack of surface expression elsewhere along the fault, suggesting that recent tectonic activity may be highly segmented or obscured by the eolian masking and erosion.

Directly NNE of the disturbed sediments detected by Radulov et al. [14] in the Skat floodplain, the Byala Slatina Depression (Figure 2) serves as a focal point for long-term tectonic subsidence associated with the central portion of the Devene fault system. This structural depocenter exhibits profound vertical displacement, with the Carboniferous strata reaching a maximum depth of 7.1 km [3]. The magnitude of this subsidence is further evidenced by Miocene deposits reaching thicknesses of approximately 700 m [26,64], suggesting that the central Devene fault system has functioned as a principal driver of regional subsidence at least during the Miocene. The spatial proximity between this Miocene maximum and the Quaternary deformation in the Skat River floodplain [14] suggests a persistent tectonic locus. While the deep subsidence of the Byala Slatina Depression defines the long-term structural maturity of the Devene system, the coseismic evidence in the Skat sector provides a data point, demonstrating that the crustal-scale architecture established during the Miocene remains, or has been revived as, a primary driver of modern fault strain release. Consequently, the western reach of the eastern fault segment appears to be the primary locus of contemporary deformation. In this zone, inherited subsidence patterns are likely manifesting as distributed, near-surface strain rather than discrete surface rupture.

Analysis of the Miocene sedimentary base within the Moesian Platform reveals a significant lateral shift in the paleo-Iskar River course relative to its contemporary Quaternary valley [26,27]. The incision of this paleovalley into the platform exceeds 200 m, providing a distinct stratigraphic marker that records approximately 20 km of cumulative lateral displacement along the eastern segment of the Devene fault system [26,27]. In the absence of precise geochronological constraints for the onset of faulting or the initiation of the paleo-Iskar drainage, the commencement of Miocene deposition (ca. 16–13 Ma) is adopted as a conservative benchmark. Utilizing this temporal baseline allows for the calculation of a maximum long-term fault slip rate that accounts for the total cumulative displacement while acknowledging the deep-seated structural inheritance of the system. This 20 km lateral offset implies an approximate maximum long-term left-lateral slip rate

of 0.14–0.19 mm/yr when averaged from the Middle Miocene to the present. The striking absence of identifiable laterally displaced landforms in the modern topography suggests a non-linear kinematic history. Fault slip rates may have been higher during the Miocene and subsequently decelerated during the Quaternary. Recent deformation may have transitioned into an increasingly blind or distributed mode. This potential deceleration, combined with the burial of the fault top beneath eolian and fluvial cover, effectively explains why the significant cumulative Miocene displacement is not mirrored by discrete ruptures in the Quaternary loess and fluvial successions. Consequently, the topographic lineaments and valley asymmetries observed today are more likely the result of climatic and lithological inheritance, as seen in the "mega-yardangs" of the Pannonian Basin [60], rather than an expression of contemporary fault activity.

5.3. Implications for SHA

If the Devene fault system is modeled as a single, continuous structure, its total length of approximately 70 km would theoretically support large-magnitude earthquakes. Based on empirical scaling laws [65,66], a rupture of this length could yield estimated magnitudes of $M_w \approx 7.0$–7.3 (Table 2). However, our findings suggest that a full-length rupture is highly improbable. Modern seismic data indicate that the seismogenic crust in this region is unlikely to exceed 10 km [15], which significantly limits the available rupture area.

Table 2. Comparison of estimated maximum moment magnitude (M_w) for the Devene fault system based on different empirical scaling constraints.

Scaling Parameter	Value	Relationship	Est. M_w	Reference
Total Fault Length (L)	≈70 km	$M_w(L)$	7.0–7.3	[65,66]
Rupture Area (A) [1]	710–745 km^2	$M_w(A)$	6.8–6.9	[67]
Displacement (D) [2]	>2–3 m	$M_w(D)$	>7.0	[65]

[1] Calculated assuming a seismogenic thickness of 10 km and a dip of 70–80°. [2] Required average displacement to reach $M_w > 7.0$ given the area constraint.

For a 70 km-long fault with a 70–80° dip angle restricted to the upper 10 km of the crust, the available rupture area is approximately 710–745 km^2. When M_w is calculated based on this area constraint [67], the estimated magnitude decreases to $M_w \approx 6.8$–6.9 (Table 2). Reaching a $M_w > 7.0$ within such a shallow seismogenic thickness would require anomalous average displacements exceeding 2–3 m, which are generally inconsistent with the distributed strain observed in the region. Following the framework of Basili et al. [11,12], Kastelic et al. [68], the Devene fault should likely be characterized as a "hidden" or "buried" source in SHA models. In such a model, the probability of surface rupture is low, but the potential for moderate-to-strong ground shaking from blind transpressional or strike–slip earthquakes remains significant. Buried ruptures can generate larger ground-motion amplitudes than surface-rupturing events of the same magnitude because they are characterized by higher dynamic stress drops and a lack of energy dissipation through surface-breaking processes [69,70]. Thus, a buried $M_w \approx 6.9$ event could potentially generate peak ground accelerations comparable to those of larger, surface-rupturing earthquakes.

Our results reinforce the need for high-resolution geophysical site investigations to differentiate between climatic landforms (e.g., remnants of linear loess dunes, asymmetric river valleys) and true tectonic features. Relying solely on surface geomorphology in loess-covered regions risks overestimating active fault density and associated seismic hazards. Moving forward, an integrated geophysical–geological approach that incorporates techniques such as seismic noise measurements (Horizontal-to-Vertical Spectral Ratio),

ground-penetrating radar, and seismic reflection would be instrumental in detecting subtle tectonic deformations within the Quaternary cover and connectivity with deeper structures. Although recent geophysical surveys have been interpreted as suggesting potential deformation elsewhere along the Devene fault system [14], these findings rely on indirect subsurface imaging and currently lack definitive geological confirmation. Hence, these results must be treated as preliminary. Definitive confirmation of Quaternary activity requires direct paleoseismologic evidence obtained through trenching techniques to identify primary surface-rupture features and provide absolute geochronological constraints.

6. Conclusions

Our investigation of the Devene fault system provides a critical re-evaluation of its Quaternary activity and regional seismic hazard. By integrating high-resolution electrical resistivity profiling with geomorphic analysis, we conclude the following:

- The geophysical surveys at Tri Kladentsi and Beli Breg confirm the presence of a steeply dipping structural boundary within the Miocene basement. At Tri Kladentsi, this is expressed as a 10 m wide vertical transition zone juxtaposing Miocene limestone against sands. At Beli Breg, the Cretaceous–Miocene contact is clearly imaged, though it appears as an erosional paleoslope without evidence of Quaternary propagation.
- Despite the deep-seated structural control, no discrete fault-related displacements were identified within the overlying Quaternary loess or fluvial successions. The sub-horizontal geometry of the loess base at Tri Kladentsi and the continuous, stacked channel sequences within the flow deflection zone at Beli Breg suggest that vertical fault displacement is either absent or negligible. Furthermore, the lack of lateral offsets or linear features within these Quaternary sediments indicates that strike–slip displacement is also unlikely, or remains below the detection limits of the high-resolution geophysical method employed.

The Devene Fault system represents a persistent, crustal-scale structure that functioned as a primary driver of lateral displacement and subsidence in the periphery of the Moesian Platform during the Miocene. The 7.1 km deep Byala Slatina Depression and the 20 km lateral offset of the paleo-Iskar River provide definitive evidence of its long-term structural maturity. Furthermore, the spatial proximity of recent coseismic deformation in the Skat River floodplain to this ancient depocenter suggests that the fault may remain active or has undergone recent reactivation, at least within its central portions. However, in the absence of direct paleoseismologic ground-truthing, such a reactivation remains a hypothesis that must be weighed against the possibility of non-tectonic factors.

Our analysis indicates a significant shift in the fault behavior over geological time. The long-term fault slip rate of 0.14–0.19 mm/yr calculated since the Miocene stands in contrast to the lack of discrete surface ruptures in the Quaternary deposits. This suggests a non-linear history that is characterized by either a deceleration of the fault slip rate or a transition into an increasingly blind and distributed deformation mode. The absence of identifiable displacements at the Tri Kladentsi and Beli Breg sites reinforces the interpretation that modern strain is absorbed by the thick Quaternary cover rather than producing discrete surface breaks.

The asymmetric valleys previously cited as tectonic evidence are more robustly explained by climatic and lithological inheritance. Dominant W–WNW paleowinds during the Quaternary drove differential loess accumulation and subsequent river channel migration, creating “pseudo-tectonic” landforms. This morphological mimicry, analogous to the eolian-sculpted “mega-yardangs” of the Pannonian Basin, demonstrates that surface geomorphology in loess-mantled regions is an unreliable proxy for active faulting and tends to overestimate fault density.

The Devene fault should be characterized as a "hidden" or "buried" source in future SHA models. Physical constraints on the seismogenic crust, which does not exceed 10 km in depth, effectively limit the maximum earthquake potential. The area-constrained magnitude is more likely restricted to $M_w \approx 6.8$–6.9. Consequently, the primary seismic risk in the region is associated with moderate-to-strong ground shaking from blind events rather than surface-rupturing earthquakes.

Author Contributions: Conceptualization, A.R.; methodology, A.R.; validation, I.A.; investigation, A.R., Y.D., N.N., M.Y., K.K. and I.A.; resources, N.N. and K.K.; data curation, I.A., Y.D. and A.R.; writing—original draft preparation, A.R.; writing—review and editing, Y.D., K.K. and M.Y.; visualization, A.R. and I.A.; project administration, A.R. and Y.D.; funding acquisition, A.R. All authors have read and agreed to the published version of the manuscript.

Funding: This study has been performed with the financial assistance of the European Union–NextGenerationEU. Project No. BG-RRP-2.0011-0010.

Data Availability Statement: The electrical resistivity datasets (BERT format) and processing configuration files used in this study are openly available in Zenodo at Radulov et al. [71], accessible via https://doi.org/10.5281/zenodo.19108088. The GNSS velocity field and seismic catalog data are available from the cited sources [4,6].

Acknowledgments: The authors would like to express their gratitude to three anonymous reviewers for their constructive comments and insightful suggestions, which significantly improved the quality of this manuscript. Figures in this manuscript were generated using the Generic Mapping Tools (GMT) 6.3 software [72]. The authors have reviewed and edited the output. All responsibility for the content of this paper is borne by the authors, and the views expressed herein can in no way be taken to reflect the official opinion of the European Union and the Bulgarian Academy of Sciences.

Conflicts of Interest: The authors declare no conflicts of interest.

Abbreviations

The following abbreviations are used in this manuscript:

BERT	Boundless Electrical Resistivity Tomography
GMT	Generic Mapping Tools
GNSS-RTK	Global Navigation Satellite System–Real-Time Kinematic
MIS	Marine Isotope Stage
MNQ	Mammal Neogene-Quaternary (zones)
RRMS	Relative Root Mean Square
SHA	Seismic Hazard Assessment

References

1. Tzankov, T.; Atanasov, A.; Bokov, P.; Vitanova, N. The Devene nappe—An Example of Local Overthrusting in the Balkanides. *Geotecton. Tectonophys. Geodyn.* **1979**, *8–9*, 93–111. (In Bulgarian)
2. Atanassov, A. Formation of the Devene Thrust. *Rev. Bulg. Geol. Soc.* **1980**, *41*, 22–32. (In Bulgarian)
3. Bokov, P.; Vassileva, A. Structural-Teclonic Peculiarities of North West Bulgaria. *Geol. Balc.* **1989**, *19*, 3–20.
4. D'Agostino, N.; Métois, M.; Koci, R.; Duni, L.; Kuka, N.; Ganas, A.; Georgiev, I.; Jouanne, F.; Kaludjerovic, N.; Kandić, R. Active Crustal Deformation and Rotations in the Southwestern Balkans from Continuous GPS Measurements. *Earth Planet. Sci. Lett.* **2020**, *539*, 116246. [CrossRef]
5. Tozer, B.; Sandwell, D.T.; Smith, W.H.F.; Olson, C.; Beale, J.R.; Wessel, P. Global Bathymetry and Topography at 15 Arc Sec: SRTM15+. *Earth Space Sci.* **2019**, *6*, 1847–1864. [CrossRef]
6. International Seismological Centre. On-Line Bulletin. 2025. Available online: http://www.isc.ac.uk/iscbulletin/search/ (accessed on 27 February 2025).
7. Reilinger, R.; McClusky, S.; Paradissis, D.; Ergintav, S.; Vernant, P. Geodetic Constraints on the Tectonic Evolution of the Aegean Region and Strain Accumulation along the Hellenic Subduction Zone. *Tectonophysics* **2010**, *488*, 22–30. [CrossRef]

8. Lazos, I.; Pikridas, C.; Chatzipetros, A.; Pavlides, S. Determination of Local Active Tectonics Regime in Central and Northern Greece, Using Primary Geodetic Data. *Appl. Geomat.* **2021**, *13*, 3–17. [CrossRef]
9. Nocquet, J.M. Present-Day Kinematics of the Mediterranean: A Comprehensive Overview of GPS Results. *Tectonophysics* **2012**, *579*, 220–242. [CrossRef]
10. Toyokuni, G.; Zhao, D. Whole-Mantle Tomography beneath Eastern Mediterranean and Adjacent Regions. *Geophys. J. Int.* **2025**, *241*, 1155–1172. [CrossRef]
11. Basili, R.; Kastelic, V.; Demircioglu Tumsa, M.B.; Garcia Moreno, D.; Nemser, E.S.; Petricca, P.; Sboras, S.P.; Besana-Ostman, G.M.; Cabral, J.; Camelbeeck, T.; et al. *European Database of Seismogenic Faults (EDSF) Compiled in the Framework of the Project SHARE*; Istituto Nazionale di Geofisica e Vulcanologia: Rome, Italy, 2013. [CrossRef]
12. Basili, R.; Danciu, L.; Beauval, C.; Sesetyan, K.; Vilanova, S.P.; Adamia, S.; Arroucau, P.; Atanackov, J.; Baize, S.; Canora, C.; et al. The European Fault-Source Model 2020 (EFSM20): Geologic Input Data for the European Seismic Hazard Model 2020. *Nat. Hazards Earth Syst. Sci.* **2024**, *24*, 3945–3976. [CrossRef]
13. Radulov, A.; Donkova, Y.; Nikolov, N.; Kostov, K.; Stefanov, Y.; Yaneva, M. Imaging the Devene Fault System beneath the Iskar Floodplain in Bulgaria through Shallow Electrical Resistivity Profiling. *Rev. Bulg. Geol. Soc.* **2024**, *85*, 31–34. [CrossRef]
14. Radulov, A.; Donkova, Y.; Yaneva, M.; Štěpančíková, P.; Tábořík, P.; Stemberk, J.; Nikolov, N.; Alexiev, I. Disturbed Sediment of the Skat Floodplain at the Intersection with the Devene Fault. *Rev. Bulg. Geol. Soc.* **2025**, *86*, 231–238. [CrossRef]
15. Kovacikova, S.; Boyadzhiev, G.; Logvinov, I. Geoelectric Studies in Earthquake Hazard Assessment: The Case of the Kozlodui Nuclear Power Plant, Bulgaria. *Nat. Hazards* **2024**, *121*, 2111–2131. [CrossRef]
16. Bončev, E. Northern Boundary of the Fore-Balkan. The Section between the Ogosta and Vit Rivers. In *Tectonics of the Fore-Balkan*; Publishing House of the Bulgarian Academy of Sciences: Sofia, Bulgaria, 1971; pp. 57–58. (In Bulgarian)
17. Čemberski, H. Concerning Certain Tectonic Problems in the Area of Boroval Hill. *Rev. Bulg. Geol. Soc.* **1961**, *22*, 283–287.
18. Stanev, I.; Berov, L. *Hydrogeological Map of People's Republic of Bulgaria. Map Sheet II–2 (Vratsa);* Committee on Geology, Scientific Research Geological Institute: Sofia, Bulgaria, 1967.
19. Yolkichev, N. Lithostratigraphic Units Related to the Upper Cretaceous in the West and Central Fore-Balkan. *Rev. Bulg. Geol. Soc.* **1986**, *48*, 49–61.
20. Ivanov, M. Notes on the Biostratigraphy of the Albian Stage between Botunja and Iskar River. *Rev. Bulg. Geol. Soc.* **1981**, *42*, 352–360.
21. Monov, B.; Nikolov, T. Lower Cretaceous Lithostratigraphy in the Western Fore-Balkan. *Rev. Bulg. Geol. Soc.* **1991**, *52*, 32–41.
22. Vangelov, D.; Gerdjikov, Y.; Kounov, A.; Lazarova, A. The Balkan Fold-Thrust Belt: An Overview of the Main Features. *Geol. Balc.* **2013**, *42*, 29–47. [CrossRef]
23. Krstekanić, N.; Matenco, L.; Stojadinovic, U.; Willingshofer, E.; Toljić, M.; Tamminga, D. Strain Partitioning in a Large Intra-continental Strike-Slip System Accommodating Backarc-Convex Orocline Formation: The Circum-Moesian Fault System of the Carpatho-Balkanides. *Glob. Planet. Change* **2022**, *208*, 103714. [CrossRef]
24. Kojumdgieva, E.; Popov, N. Lithostratigraphy of the Neogene sediments in Northwestern Bulgaria. *Palaeontol. Stratigr. Lithol.* **1988**, *25*, 3–26.
25. Kojumdgieva, E.; Popov, N. Les iignes générales de l'évolution paléogéographique de la Bulgarie du nord-ouest pendant le Néogène. *Rev. Bulg. Geol. Soc.* **1966**, *27*, 313–316.
26. Kojumdgieva, E.; Popov, N. Paleogeography and Geodynamic Evolution of Northern Bulgaria during the Neogene. *Geol. Balc.* **1989**, *19*, 73–92.
27. Spiridonov, H.; Jelev, G. Paleogeography Neogene Basins in North Bulgaria. In Proceedings of SES 2013, Sofia, Bulgaria, 20–22 November 2013 ; pp. 261–282.
28. Evlogiev, Y. *Quaternary Geology and Geomorphology of the Danube Plain. Assessment of Neotectonic Conditions at Nuclear Facilities*; Geological Institute at BAS: Sofia, Bulgaria, 2019. (In Bulgarian)
29. Evlogiev, J.; Enciu, P. Lithostratigraphic correlation of the geomorphological forms in Central North Bulgaria and South Romania. *Geol. Balc.* **2001**, *30*, 3–9. [CrossRef]
30. Minkov, M. *The Loess in North Bulgaria. A Complex Study*; Publishing House of the Bulgarian Academy of Sciences: Sofia, Bulgaria, 1968. (In Bulgarian)
31. Piña-Valdés, J.; Socquet, A.; Beauval, C.; Doin, M.P.; D'Agostino, N.; Shen, Z.K. 3D GNSS Velocity Field Sheds Light on the Deformation Mechanisms in Europe: Effects of the Vertical Crustal Motion on the Distribution of Seismicity. *J. Geophys. Res. Solid Earth* **2022**, *127*, e2021JB023451. [CrossRef]
32. Vapcarov, I.; Galabov, J.; Georgiev, M.; Vrablianski, B. Neotectonic Map of Bulgaria. In Proceedings of the Seminar on the Seismotectonic Map of the Balkan Region, Dubrovnik, Croatia, 17–26 April 1974; Volume Apendix Maps , p. 11.
33. Angelova, D. Quaternary Geology, Geomorphology and Tectonics in the Ogosta River Valley System, the Danubian Plain (Bulgaria). *Bull. Geol. Soc. Greece* **2001**, *34*, 55–60. [CrossRef]

34. Kotzev, V.; Nakov, R.; Burchfiel, B.C.; King, R.; Reilinger, R. GPS Study of Active Tectonics in Bulgaria: Results from 1996 to 1998. *J. Geodyn.* **2001**, *31*, 189–200. [CrossRef]
35. Vaptsarov, I.; Filipov, L.; Sokolova, P.; Simeonov, Y. Quaternary Geomorphology and Neotectonics of Central North Bulgaria. *Probl. Geogr.* **1993**, *3*, 18–32. (In Bulgarian)
36. Evlogiev, Y. Evidence for the Aeolian Origin of Loess in the Danubian Plain. *Geol. Balc.* **2007**, *36*, 31–39. [CrossRef]
37. Suzuki, K.; Toda, S.; Kusunoki, K.; Fujimitsu, Y.; Mogi, T.; Jomori, A. Case studies of electrical and electromagnetic methods applied to mapping active faults beneath the thick quaternary. In *Developments in Geotechnical Engineering* ; Engineering Geological Advances in Japan for the New Millennium; Kanaori, Y., Tanaka, K., Chigira, M., Eds.; Elsevier: Amsterdam, The Netherlands, 2000; Volume 84, pp. 29–45. [CrossRef]
38. Wise, D.J.; Cassidy, J.; Locke, C.A. Geophysical imaging of the Quaternary Wairoa North Fault, New Zealand: A case study. *J. Appl. Geophys.* **2003**, *53*, 1–16. [CrossRef]
39. Caputo, R.; Piscitelli, S.; Oliveto, A.; Rizzo, E.; Lapenna, V. The use of electrical resistivity tomographies in active tectonics: Examples from the Tyrnavos Basin, Greece. *J. Geodyn.* **2003**, *36*, 19–35. [CrossRef]
40. Vanneste, K.; Verbeeck, K.; Petermans, T. Pseudo-3D Imaging of a Low-Slip-Rate, Active Normal Fault Using Shallow Geophysical Methods: The Geleen Fault in the Belgian Maas River Valley. *Geophysics* **2007**, *73*, B1–B9. [CrossRef]
41. Improta, L.; Ferranti, L.; De Martini, P.M.; Piscitelli, S.; Bruno, P.P.; Burrato, P.; Civico, R.; Giocoli, A.; Iorio, M.; D'Addezio, G.; et al. Detecting Young, Slow-Slipping Active Faults by Geologic and Multidisciplinary High-Resolution Geophysical Investigations: A Case Study from the Apennine Seismic Belt, Italy. *J. Geophys. Res. Solid Earth* **2010**, *115*, B11307. [CrossRef]
42. McCalpin, J.; Ferrario, F.; Figueiredo, P.; Livio, F.; Grützner, C.; Pisarska-Jamroży, M.; Quigley, M.; Reicherter, K.; Rockwell, T.; Štěpančíková, P.; et al. New Developments in Onshore Paleoseismic Methods, and Their Impact on Quaternary Tectonic Studies. *Quat. Int.* **2023**, *664* , 59–76. [CrossRef]
43. Sapia, V.; Villani, F.; Improta, L.; Fischanger, F.; De Martini, P.M.; Romano, V.; Materni, V.; Baccheschi, P.; Smedile, A.; Nicolosi, I.; et al. Combining 3-D Deep Electrical Resistivity Tomography with Magnetic Surveys to Investigate Complex Tectonic Basins: A Case Study From the Central Apennines Seismic Belt (Italy). *Tectonics* **2025**, *44*, e2024TC008716. [CrossRef]
44. Nappi, R.; Paoletti, V.; D'Antonio, D.; Soldovieri, F.; Di Maio, R.; La Manna, M.; Fedele, A.; Ferranti, L. Joint Interpretation of Geophysical Results and Geological Observations for Detecting Buried Active Faults: The Case of the "Il Lago" Plain (Italy). *Remote Sens.* **2021**, *13*, 1555. [CrossRef]
45. Dahlin, T.; Zhou, B. A Numerical Comparison of 2D Resistivity Imaging with 10 Electrode Arrays. *Geophys. Prospect.* **2004**, *52*, 379–398. [CrossRef]
46. Loke, M.H. *Tutorial: 2-D and 3-D Electrical Imaging Surveys*; Geotomosoft Solutions: Penang, Malaysia, 2022. Available online: www.geotomosoft.com (accessed on 27 April 2026).
47. Günther, T.; Rücker, C.; Spitzer, K. Three-Dimensional Modelling and Inversion of Dc Resistivity Data Incorporating Topography—II. Inversion. *Geophys. J. Int.* **2006**, *166*, 506–517. [CrossRef]
48. Rücker, C.; Günther, T.; Spitzer, K. Three-Dimensional Modelling and Inversion of Dc Resistivity Data Incorporating Topography—I. Modelling. *Geophys. J. Int.* **2006**, *166*, 495–505. [CrossRef]
49. Anderson, E.M. *The Dynamics of Faulting and Dyke Formation with Applications to Britain*, 2nd ed.; Oliver and Boyd: Edinburgh, UK, 1951.
50. Sylvester, A.G. Strike-slip faults. *Geol. Soc. Am. Bull.* **1988**, *100*, 1666–1703. [CrossRef]
51. Rogers, C.D.F.; Dijkstra, T.A.; Smalley, I.J. Hydroconsolidation and subsidence of loess: Studies from China, Russia and North America. *Eng. Geol.* **1994**, *37*, 83–113. [CrossRef]
52. Derbyshire, E.; Mellors, T.W. Geological and geotechnical characteristics of some loess and loessic soils from China and Britain: A comparison. *Eng. Geol.* **1988**, *25*, 135–175. [CrossRef]
53. Evstatiev, D.; Antonov, D. Loess Collapsibility Problem in Bulgaria. In Proceedings of the International Symposium on Latest Natural Disasters, Sofia, Bulgaria, 5–8 September 2005; pp. 11–17.
54. Antonov, D.; Orehova, T.; Gerginov, P. Seasonal changes of the soil-water potential in loess deposits, Northeastern Bulgaria case. *Rev. Bulg. Geol. Soc.* **2018**, *79*, 133–134.
55. Rajchl, M.; Uličný, D. Depositional Record of an Avulsive Fluvial System Controlled by Peat Compaction (Neogene, Most Basin, Czech Republic). *Sedimentology* **2005**, *52*, 601–625. [CrossRef]
56. Villani, F.; Pucci, S.; Civico, R.; De Martini, P.M.; Cinti, F.R.; Pantosti, D. Surface faulting of the 1915 Avezzano earthquake (M_w 7.0, central Italy): Morphostratigraphic and paleoseismic analysis. *Tectonophysics* **2015**, *661*, 149–161. [CrossRef]
57. Schimarda, R.; Genser, J.; Meyer, M. Geophysical and geomorphological investigation of the Mur-Mürz Fault System (Eastern Alps, Austria). *Austrian J. Earth Sci.* **2010**, *103*, 70–83.
58. Leger, M. Loess Landforms. *Quat. Int.* **1990**, *7–8*, 53–61. [CrossRef]
59. Pissart, A.; Juvign'e, E.; Geurts, M.A. L'orientation des vall'ees de la r'egion de la Basse-Meuse: Un produit de la tectonique ou de l'action des vents? *Neth. J. Geosci.* **1977**, *56*, 11–20.

60. Sebe, K.; Csillag, G.; Ruszkiczay-Rüdiger, Z.; Fodor, L.; Thamó-Bozsó, E.; Magyari, E.; Szeberényi, J. Wind-sculpted Pliocene–Quaternary landscapes in the Pannonian Basin. *Territ. Atmos. Ocean. Sci.* **2011**, *22*, 659–672.
61. Spassov, N. Biochronology and zoogeographic affinities of the Villafranchian faunas of Bulgaria and South Europe. *Hist. Nat. Bulg.* **2000**, *12*, 89–128.
62. Rook, L.; Martínez-Navarro, B. Villafranchian: The long story of a Plio-Pleistocene European large mammal biochronologic unit. *Quat. Int.* **2010**, *219*, 134–144. [CrossRef]
63. Ruszkiczay-Rüdiger, Z.; Salcher, B.; Neuhuber, S.; Csillag, G.; Wieser, A.; Fodor, L. Tectonic and climatic control on terrace formation: Coupling in situ produced ^{10}Be depth profiles and luminescence approach, Danube River, Hungary, Central Europe. *Quat. Sci. Rev.* **2016**, *131*, 127–147. [CrossRef]
64. Velev, V.; Nenov, T.; Jovčev, S. Main Features of Neotectonic Development and Characteristics of the Deep Geological Structure of Moezian Plate in between Arčar and Osăm Rivers. *Geol. Balc.* **1988**, *18*, 79–91.
65. Wells, D.L.; Coppersmith, K.J. New Empirical Relationships among Magnitude, Rupture Length, Rupture Width, Rupture Area, and Surface Displacement. *Bull. Seismol. Soc. Am.* **1994**, *84*, 974–1002. [CrossRef]
66. Leonard, M. Self-Consistent Earthquake Fault-Scaling Relations: Update and Extension to Stable Continental Strike-Slip Faults. *Bull. Seismol. Soc. Am.* **2014**, *104*, 2953–2965. [CrossRef]
67. Hanks, T.C.; Kanamori, H. A moment magnitude scale. *J. Geophys. Res. Solid Earth* **1979**, *84*, 2348–2350. [CrossRef]
68. Kastelic, V.; Radulov, A.; Glavatovic, B. Improving the Resolution of Seismic Hazard Estimates for Critical Facilities: The Database of Eastern Europe Crustal Seismogenic Sources in the Frame of the SHARE Project. In Proceedings of the 30 Convegno Nazionale GNGTS, Trieste, Italy, 14–17 November 2011; pp. 218–221.
69. Somerville, P.G. Magnitude scaling of the near fault ground motion and its dependence on step overs and fault junctions. In Proceedings of the 12th Panamerican Conference on Soil Mechanics, Cambridge, MA, USA, 22–26 June 2003.
70. Kagawa, T.; Irikura, K.; Somerville, P.G. Differences in Ground Motion and Fault Rupture Process between the Surface and Buried Rupture Earthquakes. *Earth Planet. Space* **2004**, *56*, 3–14. [CrossRef]
71. Radulov, A.; Donkova, Y.; Nikolov, N.; Yaneva, M.; Kostov, K.; Alexiev, I. Electrical Resistivity Tomography (ERT) Datasets for "Morphological Mimicry in Loess-Mantled Terrains: Re-Evaluating the Quaternary Activity of the Devene Fault". [Data Set]. Zenodo, 2026. Available online: https://zenodo.org/records/19108088 (accessed on 27 April 2026)
72. Wessel, P.; Luis, J.F.; Uieda, L.; Scharroo, R.; Wobbe, F.; Smith, W.H.F.; Tian, D. The Generic Mapping Tools version 6. *Geochem. Geophys. Geosyst.* **2019**, *20*, 5556–5564. [CrossRef]

Disclaimer/Publisher's Note: The statements, opinions and data contained in all publications are solely those of the individual author(s) and contributor(s) and not of MDPI and/or the editor(s). MDPI and/or the editor(s) disclaim responsibility for any injury to people or property resulting from any ideas, methods, instructions or products referred to in the content.